UNIVERSITY OF AMSTERDAM

UvA-DARE (Digital Academic Repository)

Absorption and amplification singularities in metasurface etalons with gain

de Gaay Fortman, Nelson; Krause, Georg Michael; Schall, Peter; Koenderink, A. Femius

DOI
10.1515/nanoph-2025-0085

Publication date
2025

Document Version
Final published version

Published in
Nanophotonics

License
CC BY

Link to publication

Citation for published version (APA):
de Gaay Fortman, N., Krause, G. M., Schall, P., & Koenderink, A. F. (2025). Absorption and amplification singularities in metasurface etalons with gain. *Nanophotonics*, *14*(13), 2317-2329. https://doi.org/10.1515/nanoph-2025-0085

General rights
It is not permitted to download or to forward/distribute the text or part of it without the consent of the author(s) and/or copyright holder(s), other than for strictly personal, individual use, unless the work is under an open content license (like Creative Commons).

Disclaimer/Complaints regulations
If you believe that digital publication of certain material infringes any of your rights or (privacy) interests, please let the Library know, stating your reasons. In case of a legitimate complaint, the Library will make the material inaccessible and/or remove it from the website. Please Ask the Library: https://uba.uva.nl/en/contact, or a letter to: Library of the University of Amsterdam, Secretariat, P.O. Box 19185, 1000 GD Amsterdam, The Netherlands. You will be contacted as soon as possible.

UvA-DARE is a service provided by the library of the University of Amsterdam (https://dare.uva.nl)
Download date:10 Sept 2026

Research Article

Nelson de Gaay Fortman, Georg-Michael Krause, Peter Schall and A. Femius Koenderink*

Absorption and amplification singularities in metasurface etalons with gain

https://doi.org/10.1515/nanoph-2025-0085
Received February 19, 2025; accepted May 1, 2025;
published online May 22, 2025

Abstract: Passive reflective metasurfaces can possess perfect absorption conditions: Singular scattering anomalies at which all impinging light is absorbed. Perfect absorption is a common yet powerful metasurface design option with applications in energy harvesting, sensing, and more. Less common is the inclusion of optical gain to the system, which can give rise to a singular condition for perfect amplification. We analyze absorption and amplification singularities in plasmon antenna metasurface etalons with gain with a simple transfer matrix model. Our etalon follows the Salisbury screen design: A metal ground plate spaced by dielectric medium from an array of resonant plasmonic scatterers. We include frequency dispersive models for gain media and discuss the limitations of time reversal symmetry arguments for relating gain singularity conditions (reflectivity poles) to the well-known perfect absorption conditions (reflectivity zeros) of metasurface etalons. We show that for metasurface etalons with both gain and loss, gain can induce both perfect absorption and gain singularities, and we describe topological constraints on their creation and annihilation. Our findings have implications for the fields of non-Hermitian photonics, parity-time symmetric scattering systems, and dynamically controllable active metasurface pixels.

Keywords: metasurface; optical gain; singular optical response

1 Introduction

Reflective metasurfaces are of considerable interest for their ability to control the reflection amplitude, phase, and absorption of optical waves [1]–[11]. A common geometry is inspired by the radio frequency concept of Salisbury and Dallenbach screens: Thin (patterned) layers at a carefully chosen distance from a metal ground plate that achieve perfect absorption of impinging waves [10], [12], [13]. In optics, this motif of metasurfaces at quarter wavelength (or similar) distances from a mirror has led to advances in reflective metasurface pixels [2], [5], [7], [9], and has been used to turn intrinsically weakly absorbing layers like two-dimensional (2D) materials into effective photodetectors [14]–[16]. The seminal paper of Chong et al. relates perfect absorption to complex frequency plane analysis of the scattering matrix of photonic structures in terms of zeros and poles: The scattering matrix eigenvectors with eigenvalues 0 and ∞ [17]. In fact, according to Krasnok et al. [18] the scattering response of a system is completely determined by such zeros and poles. By adding losses one can bring zeros from the upper half complex frequency plane onto the real frequency axis. Conversely, poles correspond to scattering resonances, and when brought to the real frequency axis by gain engineering, they become amplification singularities [19]–[21]. This understanding explains Salisbury and Dallenbach screens, more general cases of coherent perfect absorption (CPA) [18], [22]–[30], as well as of CPA lasing [18]–[20], [30]–[34]. Zeros and poles furthermore have a topological character that expresses in the phase response [28]. Recently, active tuning of metasurface response through the control of zeros and poles has received interest in numerical studies. One focus has been on the active control over absorption singularities using thermo- or electro-optical mechanisms [35],

***Corresponding author: A. Femius Koenderink**, Department of Physics of Information in Matter and Center for Nanophotonics, NWO-I Institute AMOLF, Science Park 104, 1098 XG, Amsterdam, The Netherlands; and Institute of Physics, University of Amsterdam, 1098 XH, Amsterdam, The Netherlands, E-mail: fkoenderink@amolf.nl.
https://orcid.org/0000-0003-1617-5748
Nelson de Gaay Fortman, Institute of Physics, University of Amsterdam, 1098 XH, Amsterdam, The Netherlands; and Department of Physics of Information in Matter and Center for Nanophotonics, NWO-I Institute AMOLF, Science Park 104, 1098 XG, Amsterdam, The Netherlands.
https://orcid.org/0009-0005-0338-5203
Georg-Michael Krause, Department of Physics of Information in Matter and Center for Nanophotonics, NWO-I Institute AMOLF, Science Park 104, 1098 XG, Amsterdam, The Netherlands
Peter Schall, Institute of Physics, University of Amsterdam, 1098 XH, Amsterdam, The Netherlands. https://orcid.org/0000-0003-2612-2762

Open Access. © 2025 the author(s), published by De Gruyter. This work is licensed under the Creative Commons Attribution 4.0 International License.

[36], while another has been on amplification singularity tuning by means of optical gain [37], [38]. However, actively tuned singular response of a plasmon metasurface Salisbury screen with optical gain has received little attention.

In this work, we theoretically study perfect absorption (zeros) and amplification singularities (poles) in amplifying plasmon antenna metasurface etalons, extending the Salisbury-screen analogon for perfect absorption in such structures [10] to gain. The philosophy of the work is highlighted in Figure 1: While a passive metasurface etalon (panel a) may host pairs of reflection zeros we will show that the introduction of gain can give rise both to zeros and poles, and we analyze topological constraints on these singularities. We develop a transfer matrix model [39] for metasurface etalons with loss and gain and address the emergence of zeros and poles in dependence of (1) whether gain/loss is included in the spacer layer or in the metasurface, and (2) in the lattice case, how the gain is included in the meta-atoms. Furthermore, we emphasize the importance of the numerical models used for loss and gain. An appealing viewpoint comes from the field of time-reversal and Parity-Time (PT) symmetry, where nonresonant imaginary refractive index (n'') of equal magnitude but opposite sign are associated with time-reversal, *i.e.*, an interchange of loss and gain properties. This viewpoint implies simple relations between perfect absorption and gain singularity conditions. However, we argue that the physics is crucially affected by the need to account for the physical frequency dispersion in gain media: A correct gain dispersion means that gain and loss *are not* time-reversed equivalents through sign-inversion of the imaginary part of the dielectric response. Finally, we argue that Salisbury screens with gain and loss can show real-frequency zeros and poles that are very close in parameter space, which may be interesting for dynamically controllable amplitude and phase metasurface pixels with very large dynamic range.

2 Model

In this work, we consider semi-analytical modeling of amplifying metasurface etalons in which plasmon particle lattices are held in front of a mirror, and in which gain is introduced, either in the dielectric spacer or in the particle lattice. We start by reviewing simple physical models for loss and gain materials and scatterers, before recapitulating the transfer matrix method to calculate the stack response.

2.1 Model for loss materials and scatterers

The canonical model for a plasmonic particle with loss [40] starts with the Drude model for the free electron plasma, yielding the complex-valued dielectric constant

$$\epsilon_{\text{Drude}}(\omega) = \epsilon_\infty - \frac{\omega_p^2}{\omega^2 + i\omega\gamma_p}, \tag{1}$$

where ω_p is the plasma frequency, and γ_p the Ohmic damping rate. When substituted into the Rayleigh expression for the quasi-static electric dipole polarizability of a subwavelength sphere of dielectric constant ϵ and radius r in a host of dielectric constant ϵ_{host} (we use the convention $\mathbf{p} = 4\pi\epsilon_{\text{host}}\epsilon_0\alpha\mathbf{E}$ so that polarizabilities have units of volume), one finds

$$\alpha_0(\omega) = r^3 \frac{\epsilon(\omega) - \epsilon_{\text{host}}}{\epsilon(\omega) + 2\epsilon_{\text{host}}} \tag{2}$$

displaying the well-known localized surface plasmon resonance at $\epsilon(\omega) = -2\epsilon_{\text{host}}$. When $\epsilon_\infty = \epsilon_{\text{host}}$, this resonance is exactly Lorentzian.

$$\alpha_0 = \frac{V\omega_0^2}{\omega_0^2 - \omega^2 - i\omega\gamma}. \tag{3}$$

The particle resonance frequency $\omega_0 = \omega_p/\sqrt{3\epsilon_{\text{host}}}$ and damping rate follow straightforwardly from the Drude parameters, while the oscillator strength is quantified by V

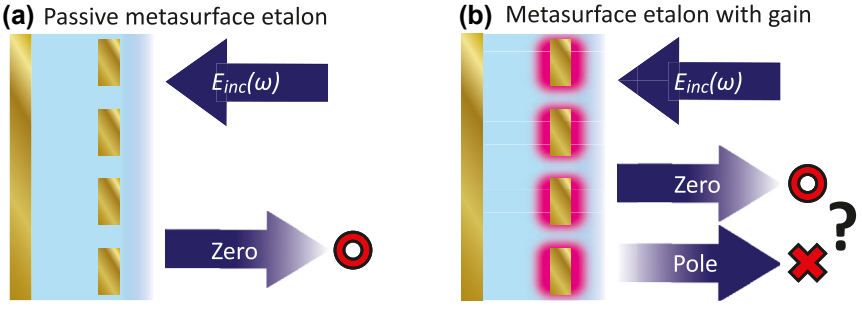

Figure 1: Singular reflection in metasurface etalons with loss and gain. (a) For a lossy, plasmon metasurface in front of a mirror, hybridization between the plasmon resonance and etalon resonances leads to pairs of perfect absorption conditions: Zeros in reflection accompanied by phase singularities in a parameter space spanned by frequency and etalon spacing. (b) When optical gain is included both reflection zeros (○) and reflection poles (×) can arise.

21928614, 2025, 13, Downloaded from https://onlinelibrary.wiley.com/doi/10.1515/nanoph-2025-0085 by Uva Universiteitsbibliotheek, Wiley Online Library on [11/05/2026]. See the Terms and Conditions (https://onlinelibrary.wiley.com/terms-and-conditions) on Wiley Online Library for rules of use; OA articles are governed by the applicable Creative Commons License

(units of volume, equal to r^3 for the Rayleigh sphere). For strong scatterers, scattering into the far-field comes with an additional loss channel. It is well known in literature [41], [42] that a self-consistent theory for multiple scattering requires to include a radiation damping factor $i2/3k^3$

$$\alpha_{\mathrm{dyn}}(\omega) = \frac{1}{1/\alpha_0 - i2/3k^3}, \tag{4}$$

where $k = n\omega/c$ is the wave number of the light in the medium surrounding the scatterer ($n = \sqrt{\epsilon_{\mathrm{host}}}$) [41], [42]. The resulting 'dynamic' polarizability satisfies the optical theorem, meaning that scattering equals extinction at zero Ohmic damping, while at non-zero Ohmic damping the extinction exceeds scattering, with the deficit equal to absorption. In this work, we start with parameters from [28], which make Eqs. (2) and (4) accurately fit finite element simulations of extinction and scattering of single nanorod plasmon antennas in glass ($n = 1.45$) for polarization along the long axis of the rods. These parameters in terms of Eq. (3) read $\omega_0 = 2.4 \times 10^{15}$ rad/s, damping rate $\gamma_p = 9.3 \times 10^{13}$ s^{-1} and $V = 6.9 \times 10^{-23}$ m^3 for Au nanorods ($100 \times 50 \times 40$ nm^3) in glass. We will vary V to control oscillator strength. Figure 2a and b show the resulting dynamic polarizability of the lossy plasmon particles. The real part shows the typical dispersive line shape, indicating the typical π phase slip in scattering that occurs upon crossing the resonance. The imaginary part is a positive Lorentzian line shape, and through the relation $\sigma_{\mathrm{ext}} = 4\pi k \mathrm{Im}\alpha_{\mathrm{dyn}}$ directly indicates the resonance in the extinction cross section.

2.2 Extension to gain materials

To describe amplifying instead of lossy scatterers, it is tempting to simply reverse the sign of the damping rate, or equivalently complex conjugate ϵ. While such a transformation has been argued to be equivalent to time reversal [43]–[48], we note that special care is required because scattering by a gainy particle is not the time-reverse of scattering by a lossy particle. Scattering redistributes light from a single input port (a plane wave) over all outgoing ports (outgoing spherical wave) at a rate given by the radiation damping term $i2/3k^3$. Time-reversing material loss into gain does not also redefine the input and output ports in a scattering problem, meaning that the radiation damping term does not change sign. Given these subtleties, it is useful to inspect gain susceptibility models and review the ramifications for scattering.

A common model in the laser community [49] to describe an inverted population of atoms in a dielectric medium is to add the susceptibility χ_{gain} of an ensemble of atoms in inversion to the background permittivity $\epsilon_b(\omega)$ as

$$\epsilon(\omega) = \epsilon_b(\omega) + \chi_{\mathrm{gain}}(\omega) \tag{5}$$

with a resonant Lorentzian lineshape

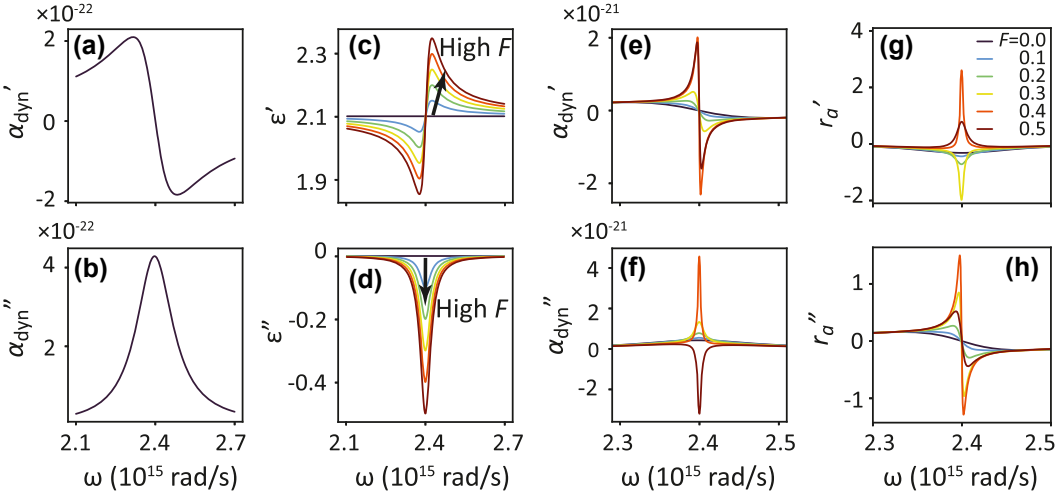

Figure 2: Response functions of lossy and gainy constituents of the plasmon metasurface etalons with gain. (a,b) Plot of Eq. (4): Real and imaginary part of the dynamic polarizability of a single plasmon rod of $V = 3 \times 10^{-23}$ m^3 (Lorentz model fitted to COMSOL simulation from Ref. [28]). (c,d) Plot of Eq. (5): Real and imaginary permittivity of a model dielectric medium with a Lorentzian gain resonance frequency $\omega_g = \omega_p = 2.4 \times 10^{15}$ rad/s, line width $\gamma_p = 0.01\omega_g$ and population inversion parameter $F = (0, 0.1, 0.2, 0.3, 0.4, 0.5)$. Note how compared to the plasmon dispersion not only the imaginary but also the real part is flipped in sign. (e,f) Plot of Eq. (4) with Eq. (5). Dynamic polarizability of a plasmon antenna coupled to a resonant gain bath according to the model of Manjavacas [50], effectively forming a combination of resonances (a,b) and (c,d). For increasing gain the sign of the metal dispersion remains, but from $F = 0.5$, $\mathrm{Im}(\alpha_{\mathrm{dyn}})$ flips sign. (g,h) Plot of Eq. (7): Reflectivity r_a of a subdiffractive ($a = 350$ nm) gain plasmonic metasurface in glass for increasing pump strength. $\mathrm{Re}[r_a]$ flips sign as the singularity condition between $F = 0.3$ and $F = 0.4$ is traversed.

21928614, 2025, 13, Downloaded from https://onlinelibrary.wiley.com/doi/10.1515/nanoph-2025-0085 by Uva Universiteitsbibliotheek, Wiley Online Library on [11/05/2026]. See the Terms and Conditions (https://onlinelibrary.wiley.com/terms-and-conditions) on Wiley Online Library for rules of use; OA articles are governed by the applicable Creative Commons License

$$\chi_{\text{gain}}(\omega) = F\frac{\gamma_g}{\omega - \omega_g + i\gamma_g}, \tag{6}$$

where ω_g is the resonant frequency of the gain medium, γ_g its line width, and F quantifies the density of excited atoms (population inversion controlled by pump strength in experiments). This model has been proposed for 3- or 4-level gain atoms [49]–[54]. Figure 2c and d plots Lorentzian susceptibility model χ_{gain} for atoms in glass, with $\omega_g = \omega_p = 2.4 \times 10^{15}$ rad/s and $\gamma_p = 0.01\omega_g$ for various pump strengths F. Importantly, the gain not only makes the imaginary part of the permittivity/polarizability negative, but also affects the dispersion in the real part of the response function. We note that a Drude scatterer can be transformed into an amplifying resonant scatterer with valid gain dispersion (as Figure 2c and d) not by $\gamma \to -\gamma$, as an intuitive time-reversal argument would suggest, but instead by $V \to -V$. Ref. [53] explains this behavior on basis of a quantum mechanical microscopic model of a 3-level atom upon pumping, from which the authors derive the classical dynamic polarizability of an atomic scatterer with gain. Below inversion, the atom dynamic polarizability displays a lossy Lorentzian polarizability, much like a plasmonic particle (panel a,b). Upon reaching population inversion, the atom becomes transparent. Crossing through transparency, the polarizability goes through zero, flipping sign both in its imaginary and real part. The sign flip in the imaginary part indicates negative extinction cross sections, i.e., amplification. The scattering cross sections $\sigma_{\text{scatt}} = 8\pi/3k^4|\alpha_{\text{dyn}}|^2$ instead remain positive.

Several works have proposed including gain into lossy plasmonic scatterers [47], [48], [50], [54]–[60]. We follow the description of Manjavacas [50], which implements gain by taking the dielectric constant of a nanoparticle as $\epsilon(\omega) = \epsilon_{\text{Drude}}(\omega) + \chi_{\text{gain}}(\omega)$, and evaluating Eq. (2) and Eq. (4). Figure 2e and f plot the real and imaginary part of the polarizability at various gain levels F. For low gain values, the polarizability is similar to that of the lossy plasmonic particle, sharpening with increasing gain as the intrinsic Drude loss is compensated. The dispersion then goes through a condition of strong scattering and strong positive extinction to a regime of negative extinction (net gain). For such a compound particle, the dispersion in the real part of polarizability *does not* flip sign.

Finally, we review how to convert the single particle polarizability into metasurface reflectivity. To calculate r_a for periodic arrays of identical scatterers, one can use Ewald lattice summation techniques that include retarded multiple scattering interactions in the point dipole approximation [42], [61]. For lattices consisting of identical scatterers specified by quasi-static polarizabilities α_0, arranged in unit cells of area A, the reflectivity in the non-diffractive regime reads

$$r_a(\omega) = \frac{2\pi ik}{A}\frac{1}{1/\alpha_0(\omega) - \frac{2\pi ik}{A}}. \tag{7}$$

Eq. (7) contains only the imaginary contribution of the lattice interaction term, as the real part induces a shift in resonance frequency which we incorporate into ω_0 [28]. Interestingly, Eq. (7) replaces the single nanoparticle radiation damping correction that is appropriate for the single scatterer (Eq. (4)) with a collective lattice damping term $2\pi ik/A$. This lattice damping term increases with antenna density and signifies superradiant damping for coherently radiating dipole arrays. [28]. In the limit of high areal density, the reflectivity approaches a perfect mirror $r_a(\omega) = -1$. In Figure 2g and h, we examine complex reflectivity of a plasmonic metasurface with gain included in α_0, according to the approach of Manjavacas [50]. The real value of r_a (Figure 2g) becomes increasingly negative with more gain, until it reaches the singular condition $\alpha_0 = A/2\pi ik$ (between $F = 0.3$ and 0.4), at which point the gain compensates the Ohmic and lattice radiation loss. At this point the reflectivity flips sign to large positive amplitudes, before converging to zero with further increase of F. Panel (h) shows that near the singularity condition, the Lorentzian curve of $\text{Im}(r_a)$ has the steepest slopes.

2.3 Metasurface etalon transfer matrix model

To describe the complete response of the composite system from the single material response just described, we use a transfer matrix method laid out in Ref. [39]. We consider normally incident radiation only. The transfer matrix method as introduced in the seminal work [62] relates parallel electric and magnetic (E, H) fields at the front side of a stack of a dielectric layer ($z = 0$) with those at the back side ($z = d_{\text{stack}}$) via multiplication of characteristic matrices of individual layers: $M_{\text{stack}} = M_N \times M_{N-1} \ldots M_2 \times M_1$ (with $m = 1, 2, \ldots N$ enumerating the layers from front to back). From the stack matrix M_{stack}, the complex reflection and transmission amplitudes follow as

$$\begin{pmatrix} t \\ ikt \end{pmatrix} = M_{\text{stack}} \begin{pmatrix} 1+r \\ ik(1-r) \end{pmatrix}. \tag{8}$$

Our stack will be composed of transfer matrices M_d for homogeneous layers of index n and thickness d, and a transfer matrix for the metasurface M_{meta}. M_d is well known in literature, but M_{meta} should depend on r_a and merits careful attention. For non-diffractive metasurfaces, M_{meta} is obtained by assuming a zero thickness layer with reflection

21928614, 2025, 13, Downloaded from https://onlinelibrary.wiley.com/doi/10.1515/nanoph-2025-0085 by Uva Universiteitsbibliotheek, Wiley Online Library on [11/05/2026]. See the Terms and Conditions (https://onlinelibrary.wiley.com/terms-and-conditions) on Wiley Online Library for rules of use; OA articles are governed by the applicable Creative Commons License

coefficient r_a, and also assuming that both slabs immediately neighboring the metasurface have identical refractive index [39]. Explicitly, M_d and M_{meta} [39] read

$$M_d = \begin{pmatrix} \cos kd & \frac{1}{k}\sin kd \\ -k\sin kd & \cos kd \end{pmatrix} \quad \text{and}$$

$$M_{\text{meta}}(r_a) = \begin{pmatrix} 1 & 0 \\ \frac{2ikr_a}{1+r_a} & 1 \end{pmatrix}. \tag{9}$$

The model does not allow for any diffraction channels, so we only consider lattices with subdiffractive pitches. We retrieve r_a from Eq. (7).

While we use the transfer matrix method for all calculations in this work, we note that for a simple two layer etalon (one mirror, one metasurface) one can extract an analytical Fabry–Perot formula [27], [28], [63]

$$r_{\text{FPI}} = \frac{r_a + r_m(1+2r_a)e^{2ik_0nd}}{1 - r_a r_m e^{2ik_0nd}}. \tag{10}$$

Here, r_m denotes the back reflector reflection coefficient. In this work, we use glass-backed gold mirrors with $n = 0.25 + 3.46i$ and thickness 50 nm or 20 nm, and dielectric spacers of varying thickness and index $n = 1.45$. Solving Eq. (8) with proper M_d, these values yield reflection coefficients $r_m = -0.5935 - 0.6502i$ and $-0.3066 - 0.5126i$, respectively. Eq. (10) has been used in literature to explain the topological constraints on perfect absorption conditions in absorbing metasurface etalons [28].

3 Results

3.1 Gain equivalent of lossy metasurface

We now discuss the response of Salisbury screens that include optical gain. We examine increasingly complex scenarios for metasurface etalons with gain, focusing on singular responses. The simplest case is presented in Figure 3: Reflectivity of a standard etalon where a lossy mirror is separated by a transparent spacer from a layer composed of nanoparticles whose response are defined by the Lorentzian Drude model (Eq. (3)). We compare the standard case of loss, modeled by positive oscillator strength V shown in panels (a-d), with the simplest self-consistent model of amplification of equivalent magnitude set by negative volume, $V \to -V$ in panels (e-h). Parameters are chosen to closely resemble the standard plasmonic Salisbury screen in Ref. [28], sketched in Figure 1a. The left three columns of Figure 3 show reflectivity amplitude in a phase space (ω, d) spanned by etalon spacing d and frequency ω, with different panels corresponding to successively higher antenna density (plots labeled with lattice pitch $a = \sqrt{A}$, assuming square lattices). The rightmost column displays reflectivity phase. Throughout this work, we use color scales for $|r_a|$ that are linear from 0 to 1 (blue to white), and logarithmic for $|r_a| > 1$ (white

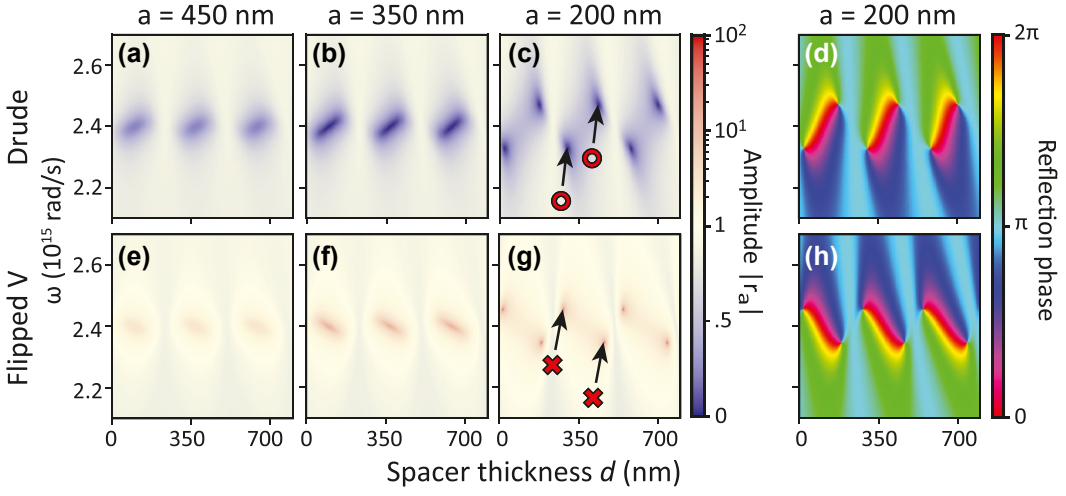

Figure 3: Transfer matrix calculations in (ω, d) space of an etalon with a regular Drude metasurface versus its amplifying equivalent. (a–c) Reflectivity amplitude for metasurfaces of increasing particle density (decreasing square arrays pitch a listed as plot titles), assuming standard lossy plasmon particles. At $a = 200$ nm, absorption zeros around the plasmon resonance appear, two of which are pointed out with a red ○ for clarity. In reflection phase ((d), referenced to same structure without particles), the pairs of zeros appear as phase singularities of opposite topological charge ±1. (e–g) Response for the amplifying equivalent structure ($V \to -V$ in Eq. (2)). Amplification singularity pairs occur at $a = 200$ nm (indicated with×). However, note that the response does not simply exchange loss for gain as also the dispersion around ω_0 is inverted. Evaluated for $V = 3 \times 10^{-23}$ m^3 and Au mirror thickness 50 nm.

21928614, 2025, 13, Downloaded from https://onlinelibrary.wiley.com/doi/10.1515/nanoph-2025-0085 by Uva Universiteitsbibliotheek, Wiley Online Library on [11/05/2026]. See the Terms and Conditions (https://onlinelibrary.wiley.com/terms-and-conditions) on Wiley Online Library for rules of use; OA articles are governed by the applicable Creative Commons License

to red, clipped at $r_a = 10^2$). Panels (a-d) show the case of a standard lossy metasurface Salisbury screen. The response is dominated by the hybridization of the antenna resonance at 2.4×10^{15} rad/s with etalon resonance conditions, especially visible in (c): At thicknesses of approximately 250, 500 and 750 nm, hyperbolic white features curve from top slightly rightward towards bottom. In between these etalon conditions, the reflectivity amplitude drops with increasing antenna density, signifying absorption. At $a = 200$ nm, the value of r_a has become large enough that points of perfect absorption occur. They arise in pairs, and coincide with singularities in the reflection phase shown in panel (d) (phase referenced to the phase pickup in absence of the particles). In the parameter space spanned by $\omega - d$, phase singularities arise in pairs of opposite charge ± 1, indicating a 2π phase increment over a (counter)clockwise loop around the singular points. These charges highlight the topological nature of the singularity conditions.

Next, we turn to the amplifying counterpart ($V \to -V$) in Figure 3e–h, the geometry of which is sketched in Figure 1b. At first glance, it appears that as loss is replaced by gain, the absorption features in reflection are replaced by enhanced reflection. At low antenna density the reflectivity enhancement is modest (mimicking the finite absorption in panels (a,b)), while above a threshold antenna density, the gain metasurface etalon displays poles in reflectivity. These emerge as the counterparts of perfect absorption in (c), and likewise correspond to phase singularities (compare panel h and d). While qualitatively the results for gain are clearly analogous to the case of loss (points of singular behavior, arising in pairs, exchanging zeros for poles), there is one striking difference: For pairs of perfect absorption the red-shifted (blue-shifted) singularity appears for spacing larger (resp. smaller) than the etalon condition, but in the case of gain this ordering is reversed. Associated with that, the phase map (h) is mirrored in the line $\omega = \omega_0$, meaning that for a given pair of singularities, not only the frequency ordering is flipped, but also the topological charges. This evidences that poles and zeros are not simply interchanged when going from a lossy polarizability to an equivalent gainy polarizability. The explanation is that the entire polarizability flips sign, i.e., both the real and imaginary parts, as opposed to complex conjugating which is common in some branches of literature on amplifying nanophotonics, *PT*-symmetry and CPA-lasing [17], [18], [30], [31], [54], [64]. In the framework of the Salisbury screen, the approach $\gamma \to -\gamma$ (leading to an amplifying but unphysical polarizability) would interchange perfect absorption for perfect amplification points, *without* rearranging the location of the singularities in phase space. The fact that a correct gain dispersion also changes the real part of the response function is well-known in other fields, such as the field of anomalous dispersion in gain media [51], [52], where the effect is responsible for superluminal light propagation.

3.2 Gainy spacers in lossy etalons

Next, we explore systems that simultaneously have both gain and loss. A first system one could envision is a standard Salisbury screen (lossy plasmonic particles), but imbuing the spacer medium with gain. We study the dependence of the Salisbury screen response on the imaginary part of the refractive index of the glass spacer layer in Figure 4, ignoring dispersion in the gain. As a starting point we take the case of Figure 3b: A Salisbury screen made with a plasmon lattice that is not quite dense enough to create points of perfect absorption if the spacer has neither gain nor loss (reproduced as panel Figure 4d). To the left of panel (d), in panels (a-c) we consider increasing loss, and to the right, in panels (e-g), increasing gain. Spacer loss/gain is modeled through a non-dispersive imaginary refractive index n'', while a constant $n' = 1.45$ defines the real part. For increasing spacer loss, we already notice for $n'' = 0.05$ that absorption singularity-pairs emerge. Their frequency separation increases with the amount of spacer loss (n'') and also with spacer thickness d. The latter effect is to be contrasted with Salisbury screens with lossless spacer: If there are singularities, they occur at all successive etalon orders and at identical frequencies, see Figure 3c and d). Turning to the case of gainy spacers in Figure 4e–g, amplification singularities appear for $n'' = -0.15$. Amplification is strongest at the etalon resonance conditions, and pockets of absorption persist. It is obvious that zeros and poles cannot simply be interchanged when $n'' \to -n''$. Indeed, it is immediately obvious that there is no time reversal symmetry when inverting the sign of n'' in the spacer, while maintaining constant particle losses.

For standard plasmonic Salisbury screens, the topological origin of perfect absorption points, and the necessity for them to occur in pairs [28], can be explained by the simple Fabry–Perot interference model Eq. (10). This analysis generalizes to the zeros and poles of amplifying metasurface etalons. Zeros arise from the numerator, and occur when the complex-valued quantities

$$z_1(\omega) = \frac{-r_a(\omega)}{1 + 2r_a(\omega)} \quad \text{and} \quad z_2(\omega, d) = r_m e^{2ik(\omega)nd} \tag{11}$$

are equal. Complex functions $z_1(\omega)$ and $z_2(\omega, d)$ are plotted in Figure 4i for a lossless spacer. The quantity z_1 is solely dependent on the metasurface. When sweeping frequency ω, z_1 traces a circle in the complex plane, starting at the

21928614, 2025, 13, Downloaded from https://onlinelibrary.wiley.com/doi/10.1515/nanoph-2025-0085 by Uva Universiteitsbibliotheek, Wiley Online Library on [11/05/2026]. See the Terms and Conditions (https://onlinelibrary.wiley.com/terms-and-conditions) on Wiley Online Library for rules of use; OA articles are governed by the applicable Creative Commons License

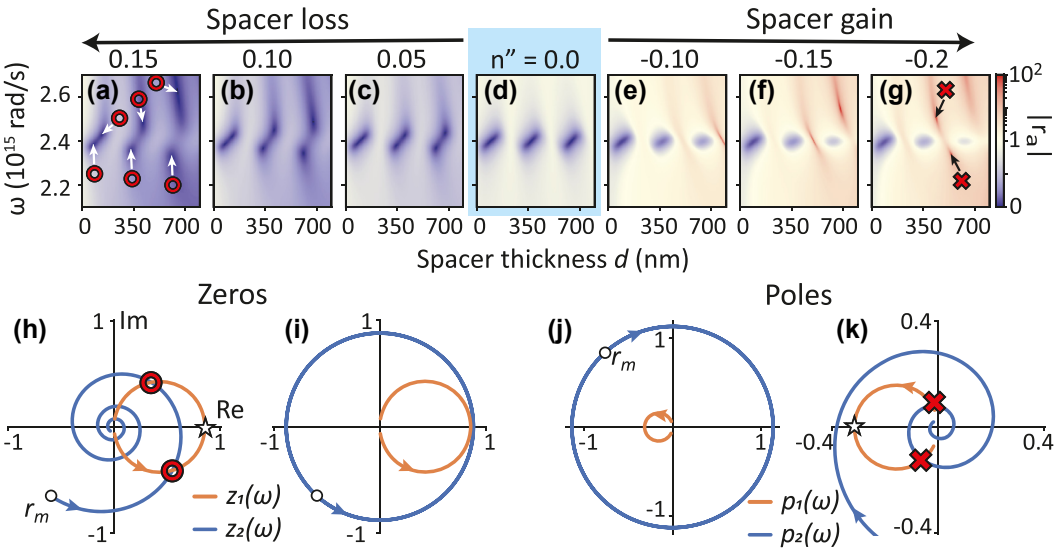

Figure 4: Response of metasurface etalons with non-dispersive loss or gain in the dielectric spacer. The metasurface comprises standard lossy plasmon antennas. (a–g) Evolution with increasing loss resp. gain of the reflection amplitude. The reference case $n'' = 0$ corresponds to panel (d). Absorption singularities appear for $n'' \geq 0.05$, and are highlighted in (a) with red ○. Reflection poles only appear for $n'' \leq -0.15$, indicated in (g) with red × for $n'' = -0.2$. (h–i) resp. (j–k) Complex-plane construction of conditions for reflection zeros resp. poles. Orange (blue) curves correspond to z_1 and p_1 (resp. z_2, p_2). Panel (h) shows how a spacer absorption of $n'' = 0.15$ generates intersections, i.e. perfect absorption points, which do not exist in the case of zero spacer loss (panel i), owing to insufficient antenna density at the chosen $a = 350$ nm. Similarly, panel (k) shows the generation of amplification singularity conditions, which only exist for sufficient spacer gain (here, $n'' = -0.2$). Evaluated for pitch $a = 350$ nm, $V = 3 \times 10^{-23}$ m^3 and Au mirror thickness 50 nm. Open black circles in (h,i) resp. (j,k) indicate r_m resp. $1/r_m$ (starting point of z_2 resp. p_2 at $d = 0$), while the asterisks indicate z_1 resp. p_1 at scatterer resonance $\omega = \omega_0$. Zeros and pole conditions are indicated by the red circles and crosses.

origin for zero frequency, returning to it at infinite frequency, while reaching its point farthest from the origin when $\omega = \omega_0$, where z_1 intersects the real axis. The circle grows in radius with increasing oscillator strength V, reaching infinite radius when $r_a(\omega_0) = -1/2$. At even stronger scattering, the circle appears on the other side of the imaginary axis. The quantity z_2 instead does not depend on the metasurface, but only on the combination of spacer and mirror. For a lossless spacer it simply traces out a circle in the complex plane of radius r_m centered on the origin, both as function of frequency ω and spacing d. For the lossless example at hand, there is no crossing between z_1 (orange curve), and z_2 (blue curve) and thus no zero reflection points are expected. For somewhat larger oscillator strength (increased radius r_a), intersections will occur in pairs and are revisited when increasing the etalon thickness d for each revolution over the blue circle.

We now discuss the generalization to lossy spacers. While the metasurface term z_1 is left unchanged, the term z_2 now changes from a circle of radius r_m to a spiral that spirals inward as the radius decreases with frequency ω and etalon spacing d. One turn of the spiral is traversed when $n'k_0 d$ corresponds to a 2π phase increment, while the change in radius per turn of the spiral is governed by n''. In panel 4h, the spiral starts at the point r_m corresponding to just the mirror, and displays already the first round trip a first pair of intersections, while the second turn generates a second pair, etcetera. The intersections correspond to points of zero reflection, and the frequency at which they occur can be read off from z_1, since each point on the orange circle corresponds to a unique frequency. The matched etalon spacing d can then be read off from z_2, since each point on z_2 corresponds to a unique value of the product ωd. The first two intersections with z_2 occur at frequencies comparatively close to the plasmon resonance. The intersections at the next higher etalon orders occur increasingly far from resonance. All these observations are in line with the transfer matrix calculations of panel (a). In the case of amplification, the spiral grows outwards, meaning that perfect absorption conditions do not occur.

A similar analysis can be made for poles in the reflectivity, for which we analyze the denominator of the Fabry–Perot interference formula. Setting the denominator to zero is equivalent to satisfying the condition $p_1(\omega) = p_2(\omega, d)$ for two complex valued quantities

$$p_1(\omega) = r_a(\omega) \quad \text{and} \quad p_2(\omega, d) = 1/(r_m e^{2ik(\omega)nd}), \qquad (12)$$

where again p_1 only depends on the metasurface response, and p_2 only depends on the mirror and spacer. Now p_1 travels a clockwise circle in the complex plane with increasing

21928614, 2025, 13, Downloaded from https://onlinelibrary.wiley.com/doi/10.1515/nanoph-2025-0085 by Uva Universiteitsbibliotheek, Wiley Online Library on [11/05/2026]. See the Terms and Conditions (https://onlinelibrary.wiley.com/terms-and-conditions) on Wiley Online Library for rules of use; OA articles are governed by the applicable Creative Commons License

frequency (panel 4j), centered on the negative real axis and touching the origin. Again, the furthest point of p_1 from the origin occurs at plasmon resonance. For $n'' = 0$, the term p_2 (a circle of radius $1/r_m$) has a much larger radius than p_1, and the system is very far from emergence of amplification singularities. As gain is introduced (panel k in Figure 4), the term p_2 turns from a circle into an inward spiral. This causes the occurrence of crossings, *i.e.*, reflection poles. The large mismatch in radius between p_1 and p_2 means that significant gain or path length is required: In this example crossings only occur at the second round trip. Higher order intersections occur but only at points very far detuned from plasmon resonance, out of the frequency range considered in our plots. Again, all observations are in line with the (ω, d) map in panel (g). To summarize, when the time-symmetry is explicitly broken, *i.e.*, introducing loss/gain in the spacer while keeping plasmon losses unchanged, very different conditions for generating zeros and poles are predicted.

3.3 Both loss and gain in metasurfaces

We finally proceed to the scenario of metasurface etalons with lossless spacers and a loss-gain metasurface, following the model of Manjavacas, where the permittivity function reads $\epsilon(\omega) = \epsilon_{\text{Drude}}(\omega) + \chi_{\text{gain}}(\omega)$ [50]. Importantly, $\text{Re}(\alpha)$ does not immediately flip sign upon increasing population inversion (Figure 2g and h). We take antenna volumes $V = 2 \times 10^{-23}\text{m}^{-3}$ and assume the gain resonance ω_g to overlap with the plasmon resonance ω_0, and take a line width $\gamma_g = 0.01\omega_g$. Figure 5 considers dense ($a = 250$ nm, panels

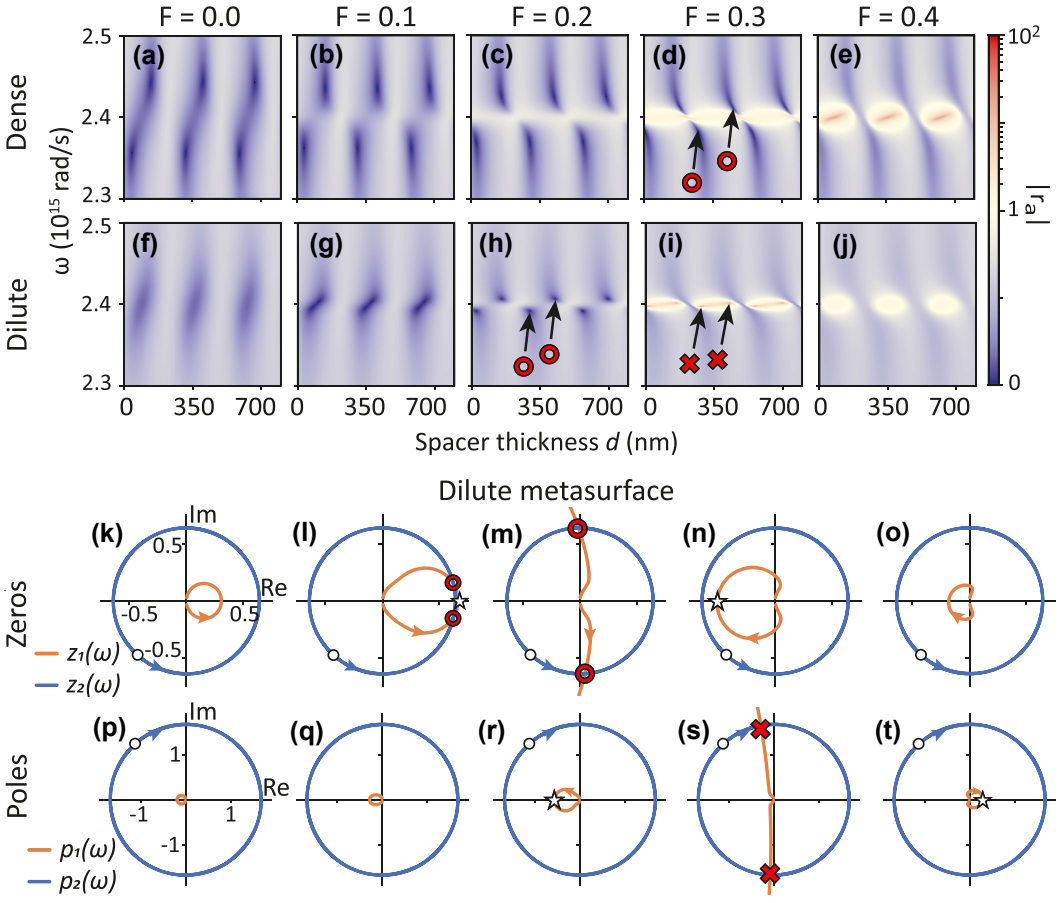

Figure 5: Response of metasurface etalons with gain-plasmon antennas, following the model of Manjavacas [50]. The spacer is lossless. (a–e) Reflectivity amplitude for a dense metasurface ($a = 250$ nm) as function of increasing gain parameter F. For $F = 0$ the absorption singularity pairs are far from the plasmon resonance. For increasing F the absorption singularities ○ approach the plasmon resonance ω_0, and ultimately disappear. (f–j) reflectivity amplitude of a dilute metasurface etalon ($a = 400$ nm), without absorption singularities in absence of gain. Absorption singularities are induced by gain (○ in panel (h), and ultimately are replaced by amplification singularities at larger gain (× in panel i). (k–o) geometrical construction in the complex plane for reflectivity zeros and poles. Orange (blue) curves correspond to z_1 and p_1 (resp. z_2, p_2). Intersections signify the occurrence of zeros (panel (m)) and poles (panel (s)). Evaluated for $V = 2 \times 10^{-23}$ m^3 and Au mirror thickness 20 nm. Open black circles in (k–o) resp. (p–t) indicate r_m resp. $1/r_m$ (starting point of z_2 resp. p_2 at $d = 0$), while the asterisks indicate z_1 resp. p_1 at scatterer resonance $\omega = \omega_0$. Zero and pole conditions are indicated by the red circles and crosses.

21928614, 2025, 13, Downloaded from https://onlinelibrary.wiley.com/doi/10.1515/nanoph-2025-0085 by Uva Universiteitsbibliotheek, Wiley Online Library on [11/05/2026]. See the Terms and Conditions (https://onlinelibrary.wiley.com/terms-and-conditions) on Wiley Online Library for rules of use; OA articles are governed by the applicable Creative Commons License

a–e) and dilute ($a = 400$ nm, panels f–j) lattices. For the dense lattice at hand, Figure 5a shows that in the absence of gain, absorption singularity pairs exist at frequencies quite far away from plasmon resonance. Increasing the gain parameter F brings the pairs closer to the resonance, until they disappear for $F = 0.4$. For the dilute lattice without gain, no absorption singularities exist (panel f), but as F increases (panels (g-j)), two absorption singularities emerge (just below $F = 0.1$). They annihilate at $F = 0.3$, when two gain singularities have emerged. Again, we can explain the singularity behavior by searching for intersections of the zero functions z_1 and z_2 in panels (a-e), and pole functions p_1 and p_2 in panels (k-o). While for the loss/gain spacer case (Figure 4), the terms z_2 and p_2 (blue curves) were modified by loss/gain, here the changes occur in the metasurface terms z_1 and p_1 (orange curves).

Focusing on the absorption zeros, if one starts with the dilute metasurface, the circle generated by z_1 is too small to generate an intersection with the term z_2 (blue circle of radius r_m). Upon pumping, loss compensation causes the metasurface response z_1 to grow in radius, creating a pair of intersections (compare panels k,l,m). Optical gain thus causes pairs of reflection zeros that will occur at all etalon orders. For further increasing gain, the singularities disappear (panel n) owing to the fact that z_1 shrinks again. It should be noted that the sharp, non-trivial dispersion causes the z_1 locus to deviate from the circular shapes that occur for simple Lorentzian antennas. Turning to the occurrence of poles one notices a similar evolution, with the locus of p_1 growing in radius in k, reaching a condition where two singularities originate in pairs (panel s), while the gain singularities disappear for even stronger pumping. For both the zero and pole construction, the trajectories of z_1 resp. p_1 change the orientation at which they cross through the real axis at critical F values. For the reflection zeros, this is associated with $\mathrm{Re}[r_a]$ crossing the value 1/2 (flipping the sign of z_1), while for the poles, this reversal occurs when $\mathrm{Re}[r_a]$) changes sign, which happens when the metasurface by itself (in absence of the back reflector) goes through its gain singularity (Figure 2g). In summary, in this type of metasurface etalon the addition of gain can induce both perfect absorption points and amplification singularities. Singularities require a critical gain: They disappear both when gain is too low and when gain is too large.

For the system with loss and gain, one may wonder if zeros and poles can coexist - or even coalesce - in (ω, d) space. In Figure 6, we focus on a small region in (ω, d) space, and very small increments of F around the emergence of gain singularities. For $F = 0.26$, the reflectivity amplitude plot (panel a) displays two perfect absorption points, as substantiated by the two oppositely charged phase singularities in the reflection phase (panel d). Here, z_1 and z_2 intersect,

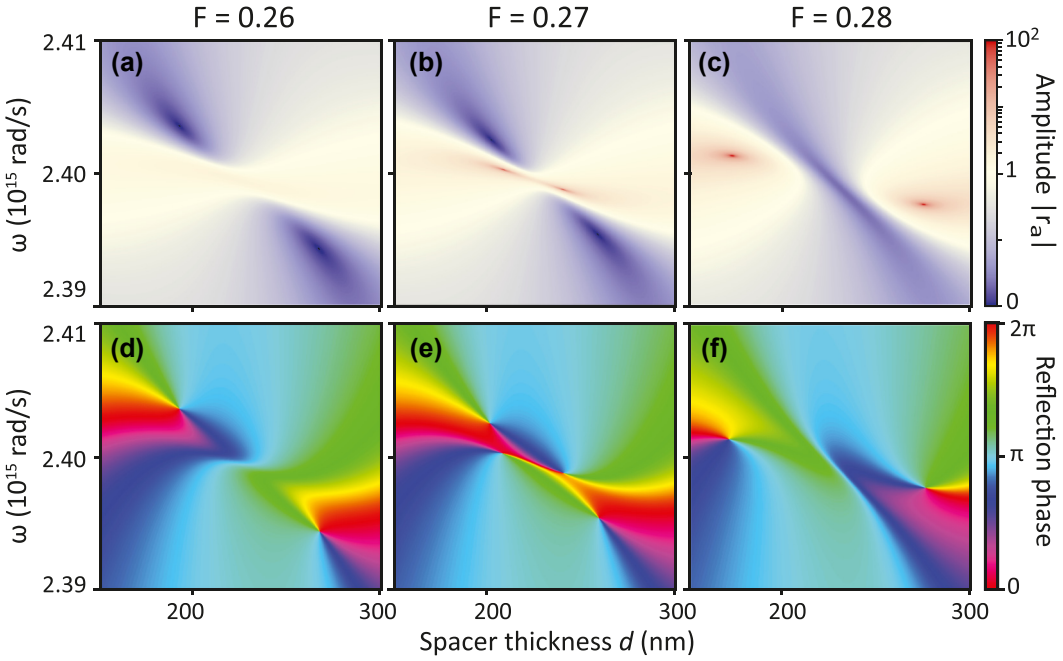

Figure 6: Birth and annihilation of absorption and amplification singularities. We consider the dilute ($a = 400$ nm) amplifying metasurface etalon of Figure 5. (a–c) and (d–f) Reflection amplitude and phase in a small part of $\omega - d$ parameter space for small increments of gain F. At $F = 0.27$ (panel b,e), both absorption and gain singularities are present, while in panels (a,d) and (c,f) only zeros resp. only poles occur. Evaluated for $V = 2 \times 10^{-23}$ m^3 and Au mirror thickness 20 nm.

21928614, 2025, 13, Downloaded from https://onlinelibrary.wiley.com/doi/10.1515/nanoph-2025-0085 by Uva Universiteitsbibliotheek, Wiley Online Library on [11/05/2026]. See the Terms and Conditions (https://onlinelibrary.wiley.com/terms-and-conditions) on Wiley Online Library for rules of use; OA articles are governed by the applicable Creative Commons License

but not p_1 and p_2. When increasing gain only very slightly to $F = 0.27$, also p_1 intersects p_2 near resonance, and two amplification singularities co-exist together with the perfect absorption points (panels b, e). Another increment in gain pushes the gain singularities away from each other, while on a trajectory in between the gain singularities, the two absorption singularities approach and annihilate ($F = 0.28$, panels c,f). The co-existence of two types of singularities in parameter space is reminiscent of Ref. [20]. One can ask if this behavior is generic, or if one can construct conditions in which the creation of the amplification singularity pair exactly coincides with the annihilation of the absorption singularity pair. Mathematically, the poles and zeros can only exactly coincide in the case of a perfect etalon, with a perfect mirror $|r_m| = 1$, and when at the same time $r_a = -1$. The latter solution from Eq. (7) implies a static polarizability $\alpha_0(\omega) = \infty$, which requires not only the usual particle plasmon resonance condition ($\mathrm{Re}[\epsilon(\omega) + 2\epsilon_{\mathrm{host}}] = 0$) to be fulfilled, but also perfect compensation of the plasmon loss by the gain [65], [66]. While this perfect mirror condition can never be strictly achieved, for very high reflectivity mirrors and antenna's operated near the polarizability singularity condition, the zero and pole may approach each other very closely in parameter space.

4 Discussion

We analyzed the physics of absorption and amplification singularities in reflectivity (in (ω, d) space) of plasmonic metasurface etalons with amplifying constituents. Several observations stand out. First, replacing plasmon antennas with pure gain counterparts is not simply a time-reversal operation in which loss singularities become gain singularities. Two aspects are at play. First, for pure gain antennas not only the imaginary part of polarizability dispersion flips sign, but also the real part. Hence singularities appear at the same equivalent oscillator strength ($|V|$), but not at the same $\omega - d$ combinations. Second, time-reversing a scattering experiment is generally not equivalent to swapping loss and gain rates, as radiation loss is not inverted in sign. A further set of peculiar observations is that (A) gain can induce perfect absorption, and (B) if gain induces poles in reflection, these conditions of singular reflection only occur at isolated (pairs of) $\omega - d$ points, (C) these generally do not persist indefinitely as gain is increased. The observation that one requires critical gain, and that *more* gain removes singular response, is reminiscent of the physics of critical coupling: Loss, gain, and coupling rates need to be all carefully matched to obtain singular response.

One has to acknowledge that in this conceptual theory work we have used gain parameters that cannot be readily obtained in optics (our values imply gain coefficients up to $g = 2 \times 10^4$ cm^{-1}). Nonetheless we argue that the phenomena may be realizable in experiments. Firstly, high gain parameters can be achieved by for instance using perovskite quantum dots [54]. Perovskite Mie scatterers that demonstrate resonant net gain and room temperature lasing have been demonstrated in literature [67], quoting $g = 3 \times 10^4$ cm^{-1} as material gain coefficient. Secondly, our model ignores near field enhancement effects that can increase gain. Lastly, one could envision using waveguiding geometries and local density of states enhancements to make better use of material gain. Indeed, these mechanisms are routinely used in plasmon lattice lasers that show modest lasing thresholds (mJ/cm^2) at material gain coefficients $g \sim 100$ cm^{-2}. We thus envision that in such systems, just below lasing threshold, application possibilities could open up as amplitude and phase tunable metasurface pixels, where each amplifying metasurface etalon forms a single pixel. The possibility to bring the absorption and amplification singularity pairs extremely close to each other in parameter space means this system can be actively tuned to switch between extreme amplitude enhancement and de-enhancement in a very small window of parameters (F, ω, d).

An open question is what the actual experimental fingerprint will be if you address the reflection poles in experiment. We have evaluated a purely linear model which should break down at the reflection pole conditions: The actual description would need to include nonlinear effects such as gain dynamics, saturation and depletion of the gain, as well as noise [54]. To account for such effects, various works employ rate equation models that incorporate both the plasmonic lattice mode and the gain medium. For the lattice interactions, either FDTD [68]–[71] or tight-binding methods [72], [73] can be used, where both routes follow density matrix methods to model the four-level gain medium. Having access to lattice plasmons coupled to gain with spatio-temporal resolution is of interest for the effect of plasmonic near fields on the gain coefficient: The plasmon mode comes with deeply subwavelength spatial and picosecond temporal signatures, and in Refs. [69], [70] it is shown that this leads to highly local gain enhancements. Although the plasmonic gain enhancements are beneficial for the amplification of a probe pulse that harvests the gain, they also lead to spatially/temporally varying gain saturation and depletion of the amplified mode [69], [70]. It remains an interesting but open question how such nonlinearities influence the dynamic behavior of light scattering

21928614, 2025, 13, Downloaded from https://onlinelibrary.wiley.com/doi/10.1515/nanoph-2025-0085 by Uva Universiteitsbibliotheek, Wiley Online Library on [11/05/2026]. See the Terms and Conditions (https://onlinelibrary.wiley.com/terms-and-conditions) on Wiley Online Library for rules of use; OA articles are governed by the applicable Creative Commons License

and lasing near the zero and pole singularities considered in this work. When operated just below lasing threshold, a small signal of probe beam could trigger the onset of lasing [69], which will occur on the pole singularity condition (ω, d) of the linear model [18]. Otherwise, temporal pulse shaping in the spirit of *virtual gain* might sidestep some of these issues, by accessing the scattering matrix at frequencies away from the real axis [18], [74]. Also, the nonlinear dynamics could open interesting perspectives for these systems as nonlinear, or self-oscillating optical elements [72], [73].

Acknowledgement: This work was part of the Dutch Research Council (NWO) and was performed at the research institute AMOLF.

Research funding: None declared.

Author contributions: NGF performed model implementation, analysis, interpretation, and writing. GMK contributed to model implementation, analysis, and interpretation. PS assisted in interpretation and commented on the manuscript. AFK contributed to model implementation, analysis, interpretation, cowriting the manuscript, and overall supervision. All authors accepted the responsibility for the content of the manuscript and consented to its submission, reviewed all the results, and approved the final version of the manuscript.

Conflict of interest: Authors state no conflict of interest.

Data availability: This paper is not associated to measured data - all graphs are obtained by plotting the quoted equations. A MATLAB code implementing the paper is available on request.

References

[1] N. I. Landy, S. Sajuyigbe, J. J. Mock, D. R. Smith, and W. J. Padilla, "Perfect metamaterial absorber," *Phys. Rev. Lett.*, vol. 100, no. 20, p. 207402, 2008.

[2] X. Liu, T. Starr, A. F. Starr, and W. J. Padilla, "Infrared spatial and frequency selective metamaterial with near-unity absorbance," *Phys. Rev. Lett.*, vol. 104, no. 20, p. 207403, 2010.

[3] K. Aydin, V. E. Ferry, R. M. Briggs, and H. A. Atwater, "Broadband polarization-independent resonant light absorption using ultrathin plasmonic super absorbers," *Nat. Commun.*, vol. 2, no. 1, p. 517, 2011.

[4] N. Yu, F. Aieta, P. Genevet, M. A. Kats, Z. Gaburro, and F. Capasso, "A broadband, background-free quarter-wave plate based on plasmonic metasurfaces," *Nano Lett.*, vol. 12, no. 12, pp. 6328—6333, 2012.

[5] A. Pors and S. I. Bozhevolnyi, "Plasmonic metasurfaces for efficient phase control in reflection," *Opt. Express*, vol. 21, no. 22, pp. 27438—27451, 2013.

[6] Y. Yao, *et al*., "Electrically tunable metasurface perfect absorbers for ultrathin mid-infrared optical modulators," *Nano Lett.*, vol. 14, no. 11, pp. 6526—6532, 2014.

[7] Y. Ra'di, C. Simovski, and S. Tretyakov, "Thin perfect absorbers for electromagnetic waves: theory, design, and realizations," *Phys. Rev. Appl.*, vol. 3, no. 3, p. 037001, 2015.

[8] F. Huang, *et al*., "Zero-reflectance metafilms for optimal plasmonic sensing," *Adv. Opt. Mater.*, vol. 4, no. 2, pp. 328—335, 2016.

[9] B. Sima, K. Chen, X. Luo, J. Zhao, and Y. Feng, "Combining frequency-selective scattering and specular reflection through phase-dispersion tailoring of a metasurface," *Phys. Rev. Appl.*, vol. 10, no. 6, p. 064043, 2018.

[10] C. M. Watts, X. Liu, and W. J. Padilla, "Metamaterial electromagnetic wave absorbers," *Adv. Mater.*, vol. 24, no. 23, pp. OP98—OP120, 2012.

[11] F. Ding, Y. Yang, R. A. Deshpande, and S. I. Bozhevolnyi, "A review of gap-surface plasmon metasurfaces: fundamentals and applications," *Nanophotonics*, vol. 7, no. 6, pp. 1129—1156, 2018.

[12] W. W. Salisbury, "Absorbent body for electromagnetic waves," US Patent, p. US2599944A, 1952.

[13] R. Fante and M. McCormack, "Reflection properties of the Salisbury screen," *IEEE Trans. Antennas Propag.*, vol. 36, no. 10, pp. 1443—1454, 1988.

[14] Y. Cai, J. Zhu, and Q. H. Liu, "Tunable enhanced optical absorption of graphene using plasmonic perfect absorbers," *Appl. Phys. Lett.*, vol. 106, no. 4, p. 043105, 2015.

[15] J. R. Piper and S. Fan, "Total absorption in a graphene monolayer in the optical regime by critical coupling with a photonic crystal guided resonance," *ACS Photonics*, vol. 1, no. 4, pp. 347—353, 2014.

[16] S. Kim, M. S. Jang, V. W. Brar, K. W. Mauser, L. Kim, and H. A. Atwater, "Electronically tunable perfect absorption in graphene," *Nano Lett.*, vol. 18, no. 2, pp. 971—979, 2018.

[17] Y. D. Chong, L. Ge, H. Cao, and A. D. Stone, "Coherent perfect absorbers: time-reversed lasers," *Phys. Rev. Lett.*, vol. 105, no. 5, p. 053901, 2010.

[18] A. Krasnok, D. Baranov, H. Li, M.-A. Miri, F. Monticone, and A. Alù, "Anomalies in light scattering," *Adv. Opt. Photon.*, vol. 11, no. 4, pp. 892—951, 2019.

[19] Z. J. Wong, *et al*., "Lasing and anti-lasing in a single cavity," *Nat. Photonics*, vol. 10, no. 12, pp. 796—801, 2016.

[20] C. Hang, G. Huang, and V. V. Konotop, "Tunable spectral singularities: coherent perfect absorber and laser in an atomic medium," *New J. Phys.*, vol. 18, no. 8, p. 085003, 2016.

[21] W. Y. Cui, J. Zhang, Y. Luo, X. Gao, and T. J. Cui, "Dynamic switching from coherent perfect absorption to parametric amplification in a nonlinear spoof plasmonic waveguide," *Nat. Commun.*, vol. 15, no. 1, p. 2824, 2024.

[22] J. Zhang, K. F. MacDonald, and N. I. Zheludev, "Controlling light-with-light without nonlinearity," *Light Sci. Appl.*, vol. 1, no. 7, p. e18, 2012.

[23] R. Alaee, M. Farhat, C. Rockstuhl, and F. Lederer, "A perfect absorber made of a graphene micro-ribbon metamaterial," *Opt. Express*, vol. 20, no. 27, pp. 28017—28024, 2012.

[24] M. Kang, Y. D. Chong, H.-T. Wang, W. Zhu, and M. Premaratne, "Critical route for coherent perfect absorption in a Fano resonance plasmonic system," *Appl. Phys. Lett.*, vol. 105, no. 13, p. 131103, 2014.

[25] M. A. Kats and F. Capasso, "Optical absorbers based on strong interference in ultra-thin films," *Laser Photonics Rev.*, vol. 10, no. 5, pp. 735—749, 2016.

[26] C. Menzel, J. Sperrhake, and T. Pertsch, "Efficient treatment of stacked metasurfaces for optimizing and enhancing the range of

21928614, 2025, 13, Downloaded from https://onlinelibrary.wiley.com/doi/10.1515/nanoph-2025-0085 by Uva Universiteitsbibliotheek, Wiley Online Library on [11/05/2026]. See the Terms and Conditions (https://onlinelibrary.wiley.com/terms-and-conditions) on Wiley Online Library for rules of use; OA articles are governed by the applicable Creative Commons License

accessible optical functionalities," *Phys. Rev. A*, vol. 93, no. 6, p. 063832, 2016.
[27] R. Alaee, M. Albooyeh, and C. Rockstuhl, "Theory of metasurface based perfect absorbers," *J. Phys. D: Appl. Phys.*, vol. 50, no. 50, p. 503002, 2017.
[28] A. Berkhout and A. F. Koenderink, "Perfect absorption and phase singularities in plasmon antenna array etalons," *ACS Photonics*, vol. 6, no. 11, pp. 2917—2925, 2019.
[29] R. Colom, *et al*., "Crossing of the branch cut: the topological origin of a universal 2π-phase retardation in non-hermitian metasurfaces," *Laser Photonics Rev.*, vol. 17, no. 6, p. 2200976, 2023.
[30] D. G. Baranov, A. Krasnok, T. Shegai, A. Alù, and Y. Chong, "Coherent perfect absorbers: linear control of light with light," *Nat. Rev. Mater.*, vol. 2, no. 1, pp. 1—14, 2017.
[31] Y. D. Chong, L. Ge, and A. D. Stone, "PT-symmetry breaking and laser-absorber modes in optical scattering systems," *Phys. Rev. Lett.*, vol. 106, no. 9, p. 093902, 2011.
[32] P. Bai, *et al*., "Simultaneous realization of a coherent perfect absorber and laser by zero-index media with both gain and loss," *Phys. Rev. A*, vol. 94, no. 6, p. 063841, 2016.
[33] B. Baum, H. Alaeian, and J. Dionne, "A parity-time symmetric coherent plasmonic absorber-amplifier," *J. Appl. Phys.*, vol. 117, no. 6, p. 063106, 2015.
[34] Z. Gu, N. Zhang, Q. Lyu, M. Li, S. Xiao, and Q. Song, "Experimental demonstration of PT-symmetric stripe lasers," *Laser Photonics Rev.*, vol. 10, no. 4, pp. 588—594, 2016.
[35] M. Elsawy, *et al*., "Universal active metasurfaces for ultimate wavefront molding by manipulating the reflection singularities," *Laser Photonics Rev.*, vol. 17, no. 7, p. 2200880, 2023.
[36] M. Li, L. Michaeli, and H. A. Atwater, "Electrically tunable topological singularities in excitonic two-dimensional heterostructures for wavefront manipulation," *ACS Photonics*, vol. 11, no. 9, pp. 3554—3562, 2024.
[37] Y.-R. Zhang, J.-Q. Yuan, Z.-Z. Zhang, M. Kang, and J. Chen, "Exceptional singular resonance in gain mediated metamaterials," *Opt. Express*, vol. 27, no. 5, pp. 6240—6248, 2019.
[38] M. Chen, Z. Li, X. Tong, X. Wang, and F. Yang, "Manipulating the critical gain level of spectral singularity in active hybridized metamaterials," *Opt. Express*, vol. 28, no. 12, pp. 17966—17978, 2020.
[39] A. Berkhout and A. F. Koenderink, "A simple transfer-matrix model for metasurface multilayer systems," *Nanophotonics*, vol. 9, no. 12, pp. 3985—4007, 2020.
[40] C. Bohren and D. R. Huffman, *Absorption and Scattering by Small Particles*, New York, John Wiley & Sons, 1983.
[41] P. de Vries, D. V. van Coevorden, and A. Lagendijk, "Point scatterers for classical waves," *Rev. Mod. Phys.*, vol. 70, no. 2, pp. 447—466, 1998.
[42] F. J. García de Abajo, "Colloquium: light scattering by particle and hole arrays," *Rev. Mod. Phys.*, vol. 79, no. 4, pp. 1267—1290, 2007.
[43] M. A. K. Othman, V. Galdi, and F. Capolino, "Exceptional points of degeneracy and PT symmetry in photonic coupled chains of scatterers," *Phys. Rev. B*, vol. 95, no. 10, p. 104305, 2017.
[44] X. Chen, W. Yue, R. Tao, P. Yao, and W. Liu, "Scattering phenomenon of PT-symmetric dielectric-nanosphere structure," *Phys. Rev. A*, vol. 94, no. 5, p. 053829, 2016.
[45] X. Chen, H. Wang, J. Li, K.-Y. Wong, and D. Lei, "Scattering asymmetry and circular dichroism in coupled PT-symmetric chiral nanoparticles," *Nanophotonics*, vol. 11, no. 9, pp. 2159—2167, 2022.
[46] C. W. Ling, K. H. Choi, T. C. Mok, Z.-Q. Zhang, and K. H. Fung, "Anomalous light scattering by topological PT-symmetric particle arrays," *Sci. Rep.*, vol. 6, no. 1, p. 38049, 2016.
[47] R. Kolkowski and A. F. Koenderink, "Lattice resonances in optical metasurfaces with gain and loss," *Proc. IEEE*, vol. 108, no. 5, pp. 795—818, 2020.
[48] R. Kolkowski, S. Kovaios, and A. F. Koenderink, "Pseudochirality at exceptional rings of optical metasurfaces," *Phys. Rev. Res.*, vol. 3, no. 2, p. 023185, 2021.
[49] A. E. Siegman, *Lasers*, Mill Valley, United States, University Science Books, 1986.
[50] A. Manjavacas, "Anisotropic optical response of nanostructures with balanced gain and loss," *ACS Photonics*, vol. 3, no. 7, pp. 1301—1307, 2016.
[51] R. Y. Chiao, "Superluminal (but causal) propagation of wave packets in transparent media with inverted atomic populations," *Phys. Rev. A*, vol. 48, no. 1, pp. R34—R37, 1993.
[52] A. Dogariu, A. Kuzmich, and L. J. Wang, "Transparent anomalous dispersion and superluminal light-pulse propagation at a negative group velocity," *Phys. Rev. A*, vol. 63, no. 5, p. 053806, 2001.
[53] T. Savels, A. P. Mosk, and A. Lagendijk, "Light scattering from three-level systems: the T matrix of a point dipole with gain," *Phys. Rev. A*, vol. 71, no. 4, p. 043814, 2005.
[54] A. Krasnok and A. Alù, "Active nanophotonics," *Proc. IEEE*, vol. 108, no. 5, pp. 628—654, 2020.
[55] A. A. Govyadinov, V. A. Podolskiy, and M. A. Noginov, "Active metamaterials: sign of refractive index and gain-assisted dispersion management," *Appl. Phys. Lett.*, vol. 91, no. 19, p. 191103, 2007.
[56] S. Campione, M. Albani, and F. Capolino, "Complex modes and near-zero permittivity in 3D arrays of plasmonic nanoshells: loss compensation using gain," *Opt. Mater. Express*, vol. 1, no. 6, pp. 1077—1089, 2011.
[57] S. Schwaiger, *et al*., "Gain in three-dimensional metamaterials utilizing semiconductor quantum structures," *Phys. Rev. B*, vol. 84, no. 15, p. 155325, 2011.
[58] N. Arnold, K. Piglmayer, A. V. Kildishev, and T. A. Klar, "Spasers with retardation and gain saturation: electrodynamic description of fields and optical cross-sections," *Opt. Mater. Express*, vol. 5, no. 11, pp. 2546—2577, 2015.
[59] V. Caligiuri, L. Pezzi, A. Veltri, and A. De Luca, "Resonant gain singularities in 1D and 3D metal/dielectric multilayered nanostructures," *ACS Nano*, vol. 11, no. 1, pp. 1012—1025, 2017.
[60] G. V. Kristanz, N. Arnold, A. V. Kildishev, and T. A. Klar, "Power balance and temperature in optically pumped spasers and nanolasers," *ACS Photonics*, vol. 5, no. 9, pp. 3695—3703, 2018.
[61] S. Baur, S. Sanders, and A. Manjavacas, "Hybridization of lattice resonances," *ACS Nano*, vol. 12, no. 2, pp. 1618—1629, 2018.
[62] P. Yeh, "Optics of anisotropic layered media: a new 4×4 matrix algebra," *Surf. Sci.*, vol. 96, no. 1, pp. 41—53, 1980.
[63] A. Kwadrin, C. I. Osorio, and A. F. Koenderink, "Backaction in metasurface etalons," *Phys. Rev. B*, vol. 93, no. 10, p. 104301, 2016.

21928614, 2025, 13, Downloaded from https://onlinelibrary.wiley.com/doi/10.1515/nanoph-2025-0085 by Uva Universiteitsbibliotheek, Wiley Online Library on [11/05/2026]. See the Terms and Conditions (https://onlinelibrary.wiley.com/terms-and-conditions) on Wiley Online Library for rules of use; OA articles are governed by the applicable Creative Commons License

[64] S. Longhi, "PT-symmetric laser absorber," *Phys. Rev. A*, vol. 82, no. 3, p. 031801, 2010.
[65] N. M. Lawandy, "Localized surface plasmon singularities in amplifying media," *Appl. Phys. Lett.*, vol. 85, no. 21, pp. 5040—5042, 2004.
[66] A. Veltri and A. Aradian, "Optical response of a metallic nanoparticle immersed in a medium with optical gain," *Phys. Rev. B*, vol. 85, no. 11, p. 115429, 2012.
[67] E. Tiguntseva, *et al*., "Room-temperature lasing from mie-resonant nonplasmonic nanoparticles," *ACS Nano*, vol. 14, no. 7, pp. 8149—8156, 2020.
[68] A. Fang, T. H. Koschny, and C. M. Soukoulis, "Self-consistent calculations of loss-compensated fishnet metamaterials," *Phys. Rev. B*, vol. 82, no. 12, p. 121102(R), 2010.
[69] S. Wuestner, A. Pusch, K. L. Tsakmakidis, J. M. Hamm, and O. Hess, "Gain and plasmon dynamics in active negative-index metamaterials," *Phil. Trans. R. Soc. A.*, vol. 369, no. 1950, pp. 3525—3550, 2011.
[70] O. Hess, J. B. Pendry, S. A. Maier, R. F. Oulton, and K. L. Tsakmakidis, "Active nanoplasmonic metamaterials," *Nat. Mater.*, vol. 11, no. 7, pp. 573—584, 2012.
[71] J. Cuerda, F. Rüting, F. J. García-Vidal, and J. Bravo-Abad, "Theory of lasing action in plasmonic crystals," *Phys. Rev. B*, vol. 91, no. 4, p. 041118(R), 2015.
[72] J.-S. Wu, V. Apalkov, and M. I. Stockman, "Topological spaser," *Phys. Rev. Lett.*, vol. 124, no. 1, p. 017701, 2020.
[73] N. de Gaay Fortman, R. Kolkowski, D. Pal, S. R. K. Rodriguez, P. Schall, and A. F. Koenderink, "Spontaneous symmetry breaking in plasmon lattice lasers," *Sci. Adv.*, vol. 10, no. 27, p. eadn2723, 2024.
[74] D. G. Baranov, A. Krasnok, and A. Alù, "Coherent virtual absorption based on complex zero excitation for ideal light capturing," *Optica*, vol. 4, no. 12, pp. 1457—1461, 2017.

21928614, 2025, 13, Downloaded from https://onlinelibrary.wiley.com/doi/10.1515/nanoph-2025-0085 by Uva Universiteitsbibliotheek, Wiley Online Library on [11/05/2026]. See the Terms and Conditions (https://onlinelibrary.wiley.com/terms-and-conditions) on Wiley Online Library for rules of use; OA articles are governed by the applicable Creative Commons License